

## Rietveld refinement of the todorokite structure

JEFFREY E. POST

Department of Mineral Sciences, Smithsonian Institution, Washington, D.C. 20560, U.S.A.

DAVID L. BISH

Earth and Space Sciences Division, Los Alamos National Laboratory, Los Alamos, New Mexico 87545, U.S.A.

### ABSTRACT

Rietveld refinements, using powder X-ray data, of the structures of todorokite samples from South Africa and Cuba have confirmed the basic  $[3 \times 3]$  tunnel structure and, for the first time, have provided information about the positions of the tunnel cations and water molecules. Fourier-difference maps and subsequent refinements show a major tunnel site at about  $(0.36, 0, 0.35)$  and smaller more diffuse areas of electron density near  $(0.70, \frac{1}{2}, 0.38)$  and  $(\frac{1}{2}, \frac{1}{2}, \frac{1}{2})$ . Structure-energy calculations suggest that the first two positions are occupied by water molecules and the third by cations such as Na and Ca. The difference maps indicate considerable positional disorder on the tunnel sites, probably caused by various tunnel contents and configurations of lower-valence octahedral cations in different unit cells. The Mn<sub>2</sub>O octahedra at the edges of the triple chains have larger mean Mn–O distances and probably accommodate the larger cations found in todorokite, e.g., Mg<sup>2+</sup>, Mn<sup>3+</sup>, Cu<sup>2+</sup>, Ni<sup>2+</sup>, etc.

### INTRODUCTION

The crystal structure of todorokite has been a subject of interest and speculation for several decades. Much of this attention stems from its role as a major manganese oxide phase in ocean manganese nodules and the possibility that it is the host for Cu, Ni, and other important metals found in the nodules (Burns et al., 1983). Todorokite also occurs in many terrestrial manganese deposits and in some cases is mined as an ore of manganese. Recently, studies have shown that todorokite exhibits dehydration and cation-exchange behavior similar to many zeolites, suggesting possible potential as a catalyst material (Bish and Post, 1984). Unfortunately, like many other tetravalent manganese oxide minerals, todorokite typically occurs as poorly crystalline masses, and to date no crystals have been found that are suitable for single-crystal X-ray or neutron-diffraction studies. Consequently, many questions remain about the crystal chemistry and structure of todorokite.

Todorokite is a hydrated Na-, Ca-, K-, Mg-bearing manganese oxide with characteristic X-ray powder-diffraction lines at about 9.6, 4.8, and 2.42 Å. Chemical analyses (e.g., Ostwald, 1986) show a wide range of compositions and suggest the general formula  $(\text{Na,Ca,K,Ba,Sr})_{0.3-0.7}(\text{Mn,Mg,Al})_6\text{O}_{12} \cdot 3.2-4.5\text{H}_2\text{O}$ . For many years, a controversy existed in the literature about the nature of the todorokite crystal structure. On the basis of electron-diffraction data and the commonly fibrous habit, Burns and Burns (1977) proposed a tunnel structure for todorokite, similar to those of the tetravalent manganese oxide minerals romanechite and hollandite. On the other hand, infrared-spectroscopy data and the

sometimes platy habit exhibited by todorokite supported the notion of a layer structure, analogous to birnessite (Potter and Rossman, 1979). A third point of view expressed by Giovanoli and coworkers (e.g., Giovanoli and Burki, 1975) maintained that todorokite was in fact not a valid mineral species but rather a mixture of buserite and/or birnessite and manganite.

In recent years, speculations about the basic todorokite structure have largely been laid to rest by high-resolution transmission electron microscopy (HRTEM) studies that confirm the tunnel model proposed by Burns and Burns (1977) (Chukhrov et al., 1978; Turner and Buseck, 1981). The HRTEM images reveal that todorokite consists predominantly of triple chains of edge-sharing Mn<sub>2</sub>O octahedra that corner-share to form large tunnels, measuring three octahedra on a side  $[3 \times 3]$  (Fig. 1). The unit cell nominally has six Mn and 12 O atoms constituting the octahedral framework, along with the tunnel cations and water molecules. The todorokite structure is similar to those of hollandite and romanechite but has larger tunnels. Hollandite is constructed of double chains of Mn<sub>2</sub>O octahedra forming  $[2 \times 2]$  tunnels, and romanechite of double and triple chains, resulting in  $[2 \times 3]$  tunnels. The HRTEM images of the todorokite structure commonly show intergrowths of larger tunnels, e.g.,  $[3 \times 4]$  and  $[3 \times 5]$ , with the basic  $[3 \times 3]$  units (Chukhrov et al., 1978; Turner and Buseck, 1981). Unfortunately, the HRTEM studies cannot provide precise atom positions and bond lengths for todorokite, nor do they give any information about the locations of the cations (Na, Ca, K, etc.) and water molecules that presumably reside in the large tunnels.

Because of the difficulty (and perhaps impossibility) of

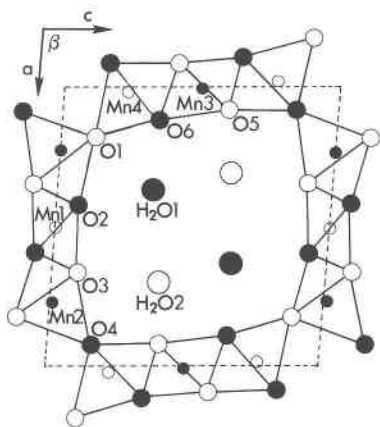


Fig. 1. Projection of the Rietveld-refined todorokite structure down  $b$ . The filled circles represent atoms at  $y = 0$ , and the open circles, those at  $y = \frac{1}{2}$ .

obtaining todorokite crystals suitable for single-crystal diffraction experiments, we have attempted to refine the crystal structure of todorokite by the Rietveld method (Rietveld, 1969), using X-ray powder-diffraction data. In addition to confirming the  $[3 \times 3]$  tunnel structure indicated by HRTEM studies, a major goal of this study has been to locate the positions of the tunnel cations and water molecules.

Generally, there are two approaches used to extract structural information from X-ray powder-diffraction data. In the first method, the powder-diffraction pattern is decomposed into the component Bragg reflections, and the integrated intensities are measured. These Bragg intensities, after correction for multiplicity and Lorentz-polarization effects, are used in the same manner as those determined by single-crystal experiments. This so-called profile-fitting procedure works well for relatively simple structures that yield powder patterns having mostly resolved Bragg peaks. In the case of todorokite, however, there are no completely resolved reflections in the range  $8^\circ$  to  $130^\circ 2\theta$ . In fact, most of the peaks in the todorokite powder pattern (Figs. 2 and 3) are composed of from several to up to a dozen or more Bragg reflections. It would be extremely difficult, if not impossible, to use a profile-fitting procedure on the todorokite powder X-ray pattern. Fortunately, the Rietveld approach does not require determination of individual Bragg intensities. Instead, each data point in the powder profile is used as an observation in the structure refinement (Rietveld, 1969). A limitation of the Rietveld method is that one must start with a model that is a reasonable approximation of the actual structure. Typically, a starting model is conceived by analogy to similar structures, by distance-least-squares (DLS) (Villiger, 1969) calculations, or as in the case of todorokite, from HRTEM studies. In the actual refinement procedure, the atom positions, occupancies, unit-cell parameters, and background coefficients, along with profile parameters such as half-widths, peak asymmetry, etc., are varied in a least-squares procedure until the calculated

powder profile, based on the structure model, best matches the observed pattern. The Rietveld method has been used successfully in recent years to refine several structures, using neutron or X-ray powder data (e.g., Thompson and Wood, 1983; Hill, 1984; Hill and Madsen, 1984; Baerlocher, 1984). Most previous Rietveld refinements using X-ray data have involved relatively simple structures with few variable parameters; todorokite should provide a more severe test of the technique.

### EXPERIMENTAL DETAILS

The two todorokite samples used in this study are from the N'Chwaning Mine, North Cape Province, South Africa (Harvard University no. 126232), and Charco Redondo, Cuba (Harvard University no. 106238). Both samples show a fibrous habit. Electron-microprobe (South African sample) and wet-chemical (Cuban sample) analyses yield the following chemical formulae: South Africa— $(\text{Na}_{0.40}\text{Ca}_{0.14}\text{K}_{0.01})(\text{Mn}_{5.71}^{4+}\text{Mg}_{0.43})\text{O}_{12} \cdot 4.59\text{H}_2\text{O}$ ; Cuba— $(\text{Na}_{0.27}\text{Ca}_{0.22}\text{K}_{0.06}\text{Sr}_{0.03}\text{Ba}_{0.01})(\text{Mn}_{5.34}^{4+}\text{Mg}_{0.44}\text{Al}_{0.02}\text{Fe}_{0.01})\text{O}_{12} \cdot 3.1\text{H}_2\text{O}$ . The water values were determined using a Dupont 903H moisture-evolution analyzer.

Samples for X-ray powder diffraction were ground in an agate mortar to less than 400 mesh and front-loaded into a cavity-type sample holder. The data for the samples from South Africa and Cuba were collected in the step-scan mode using a Scintag and Siemens automated X-ray powder diffractometer, respectively. Data-collection parameters for the two samples are listed in Table 1. The sample from South Africa was repacked and rerun three times at a scan rate of  $1^\circ/\text{min}$  to check for evidence of preferred orientation. No significant changes in intensities were noticed among the three data sets, suggesting that preferred orientation effects are minimal. The powder patterns for the Cuban and South African samples show minor impurities of quartz, and quartz and calcite, respectively.

For all of the refinements, the data in the low-angle range (see Table 2) were excluded because in this region not all of the incident X-ray beam is striking the sample and therefore relative observed intensities are too low. Also,  $2\theta$  regions (see Table 2) encompassing the strongest lines for quartz and calcite were excluded from the data.

### REFINEMENT AND FOURIER ANALYSIS

The observed X-ray powder profiles for the two todorokite samples are plotted in Figures 2 and 3. It is obvious that most of the peaks in the two patterns appear relatively broad ( $\text{FWHM} > 0.5^\circ$  at  $30^\circ$ ), and although this broadening in part can be explained for many of the peaks by the large number of contributing Bragg reflections (note reflection markers in Figs. 2 and 3), undoubtedly some of the broadening results from structural disorder. As mentioned above, HRTEM images of the todorokite structure invariably show octahedral chains of different widths randomly intergrown with the predominant triple chains (Chukhrov et al., 1978; Turner and Buseck, 1981). Also, HRTEM images indicate that the  $\beta$  angle for different unit cells can range from  $90^\circ$  to  $110^\circ$  (Turner, 1982). Both of these structural effects probably contribute to the peak broadening in todorokite powder-diffraction patterns. Peak broadening is especially apparent in the profile for the sample from Cuba (Fig. 2). Similar broadening of certain

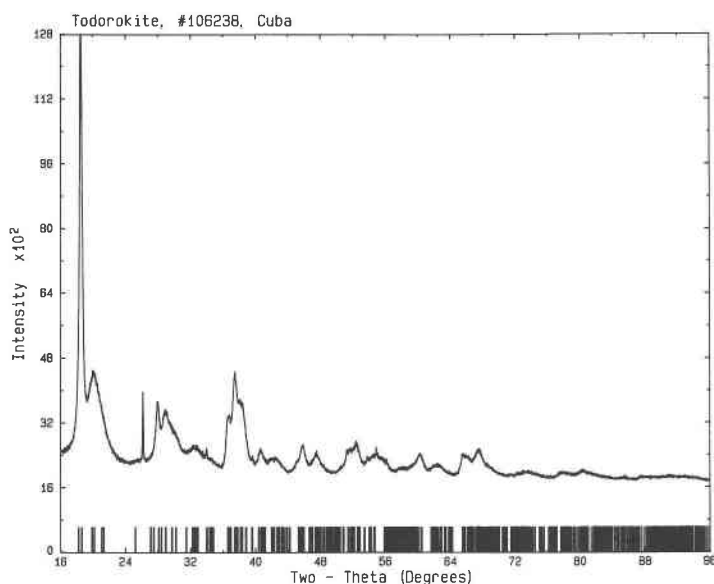


Fig. 2. Observed X-ray diffraction pattern for todorokite from Cuba, offset by one major division on the  $y$  axis (i.e., the zero-intensity point is 1600). The vertical bars mark positions of Bragg reflections.

classes of reflections is also observed in X-ray powder-diffraction patterns of hollandites and romanechite, which also show chain-width disorder in HRTEM images (Turner and Buseck, 1979). It is not known how seriously the todorokite structural disorder affects the Rietveld refinement results, but it undoubtedly contributes to a somewhat higher value for the profile residual.

The  $[3 \times 3]$  Mn<sub>3</sub>O octahedral framework shown in Figure 1 was the starting model for the Rietveld refinements

of the todorokite structure. Initial atom positions (Table 3) were determined by DLS calculations with program DLS76 (Baerlocher et al., 1977), based on observed Mn–O and O–O bond distances from single-crystal X-ray studies of romanechite and hollandite (Turner and Post, in prep.; Post et al., 1982). Unit-cell parameters for the DLS calculations were fixed to observed powder-diffraction values for the todorokite from South Africa. For both DLS modeling and subsequent Rietveld refinements, space group

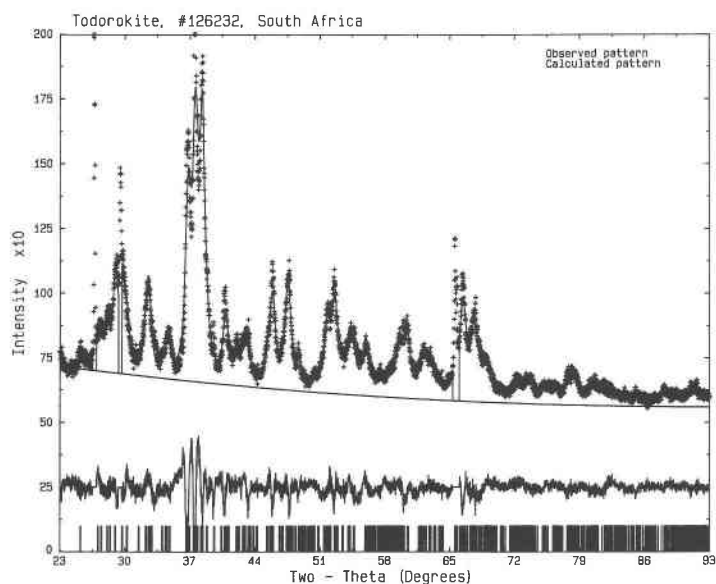


Fig. 3. Observed and calculated X-ray diffraction patterns for South African todorokite using  $\text{CuK}\alpha$  radiation. The crosses are the observed data, and the solid line is the calculated profile. The smooth line beneath the patterns is the calculated background. The patterns have been offset by two major divisions along the  $y$  axis (i.e., the zero point is at 500). The difference between the observed and calculated patterns is plotted below. The vertical bars mark all possible Bragg reflections.

TABLE 1. Data-collection parameters

	South Africa		Cuba
	CuK $\alpha$	CuK $\beta$	CuK $\alpha$
Radiation	CuK $\alpha$	CuK $\beta$	CuK $\alpha$
Detector	Solid state (Ge)		Scintillation
Monochromator	None	None	Graphite (diffracted beam)
Slits			
Primary	1 mm	1 mm	1°
Receiving	0.2 mm	0.2 mm	1°
Soller	Incident, diffracted		Incident, diffracted
Scan			
Range ( $^{\circ} 2\theta$ )	6–110	6–110	8–96
Step size ( $^{\circ} 2\theta$ )	0.02	0.02	0.02
Time/step (s)	40	40	70

$P2/m$  was assumed because it is consistent with the symmetry exhibited by the  $[3 \times 3]$  octahedral framework and with the  $2/m$  Laue symmetry shown by electron-diffraction patterns (Turner, 1982). In the absence of any positional information, tunnel cations and water molecules were excluded from DLS calculations and from initial stages of refinement.

All Rietveld refinements were carried out using the computer program DBW3.2 (Wiles and Young, 1981), as modified by S. Howard (pers. comm.). During the early stages of refinement only the following parameters were varied: scale factor, background coefficients, unit-cell parameters, full-width parameters, sample displacement, and peak asymmetry ( $< 50^{\circ} 2\theta$ ). First, only the scale factor was refined, and then gradually the remaining parameters were included in successive least-squares cycles. The background was fit using a third-order polynomial, and the observed peak shapes were approximated with a Pearson VII profile function, limited to ten full-widths on each side of the peak maximum. The Pearson VII mixing coef-

ficient was also included as a refinable profile parameter. In the case of the Cuban sample, there was difficulty refining full-width parameters, and we were forced to use a full-width that had a fixed  $2\theta$  dependence. This problem likely arose because of differences in peak widths for different classes of reflections, caused by structural disorder. Using the DLS-determined fixed Mn<sub>2</sub>O framework, the refinements converged to weighted profile residuals of 0.16, 0.17, and 0.16 for the South African K $\alpha$ , K $\beta$ , and Cuban data sets, respectively. The reasonably low  $R_{wp}$  values, at least for Rietveld refinements using X-ray data, affirm that our starting model structure is basically correct.

Refined unit-cell parameters for the two samples are listed in Table 2. For powder patterns having many overlapping reflections, as in the case of todorokite, Rietveld refinement is probably the method of choice for determining accurate unit-cell parameters. Small discrepancies between the values for the two samples are likely a manifestation of compositional differences.

In an attempt to locate the positions of the tunnel species, Fourier-difference maps were calculated using the observed Bragg intensities as determined by the Rietveld refinement procedure described above. These intensities were corrected for multiplicity and Lorentz-polarization effects and converted into structure factors for use in the XRAY76 crystallographic computing package (Stewart, 1976). Using the same DLS todorokite structure as above, an overall scale factor was refined and a three-dimensional difference-Fourier map was computed for each of the todorokite data sets, with 0.3-Å resolution. Sections from the maps are pictured in Figures 4 and 5.

When interpreting difference maps based on Rietveld intensities, it is important to consider that the results are

TABLE 2. Final Rietveld refinement parameters for todorokite

	South Africa		Cuba
	K $\alpha$	K $\beta$	
<i>a</i> (Å)	9.764(1)	9.763(2)	9.789(6)
<i>b</i> (Å)	2.8416(4)	2.8454(4)	2.834(1)
<i>c</i> (Å)	9.551(1)	9.559(1)	9.551(4)
$\beta$ ( $^{\circ}$ )	94.06(1)	94.16(1)	93.72(3)
<i>V</i> (Å <sup>3</sup> )	264.32	264.83	264.46
Pearson VII coef.	1.05(3)	1.06(3)	-0.50(6)‡
Asymmetry parameter	0.006(3)	-0.03(1)	-0.04(1)
FWHM ( $^{\circ} 2\theta$ at 30°)*	0.59	0.45	1.63
Overall <i>B</i>	0.06(8)	-0.50(8)	0.65(8)
Excluded regions ( $^{\circ}$ )	6–20	6–20	8–27
	26.5–26.9	18.6–19.0	
	29.3–29.6	22.7–22.84	
	65.3–66.0	23.84–24.18	
		26.4–26.74	
		58.38–58.78	
Parameters	36	36	35
Bragg reflections	401	549	310
$R_p$ **	0.089	0.106	0.097
$R_{wp}$ †	0.113	0.135	0.124
$R_{Bragg}$	0.046	0.054	—§

\* Full-width at one-half maximum peak height.

\*\*  $R_p = \sum_i (|I_{obs,i} - I_{calc,i}|) / \sum_i I_{obs,i}$ .

†  $R_{wp} = [\sum_i w_i (I_{obs,i} - I_{calc,i})^2 / \sum_i w_i I_{obs,i}^2]^{1/2}$ .

‡ Pseudo-voight coefficient.

§  $R_{Bragg}$  not calculated.

TABLE 3. Todorokite atom positions

		South Africa			
		DLS	$K\alpha$	$K\beta$	Cuba
Mn1	x	1/2	1/2	1/2	1/2
	y	1/2	1/2	1/2	1/2
	z	0	0	0	0
Mn2	x	0.769	0.764	0.766	0.764
	y	0	0	0	0
	z	0.002	0.002	0.001	0.002
Mn3	x	0	0	0	0
	y	0	0	0	0
	z	1/2	1/2	1/2	1/2
Mn4	x	0.978	0.974	0.975	0.990
	y	1/2	1/2	1/2	1/2
	z	0.767	0.765	0.768	0.759
O1	x	0.162	0.178	0.176	0.180
	y	1/2	1/2	1/2	1/2
	z	0.102	0.119	0.117	0.116
O2	x	0.418	0.418	0.419	0.403
	y	0	0	0	0
	z	0.096	0.079	0.066	0.069
O3	x	0.679	0.665	0.649	0.663
	y	1/2	1/2	1/2	1/2
	z	0.098	0.090	0.080	0.110
O4	x	0.920	0.917	0.932	0.908
	y	0	0	0	0
	z	0.145	0.150	0.148	0.150
O5	x	0.911	0.913	0.902	0.993
	y	1/2	1/2	1/2	1/2
	z	0.397	0.407	0.400	0.472
O6	x	0.888	0.880	0.895	0.889
	y	0	0	0	0
	z	0.657	0.649	0.653	0.666
H <sub>2</sub> O(1)	x		0.363	0.405	
	y		0	0	
	z		0.353	0.414	
H <sub>2</sub> O(2)	occ.		0.92	0.86	
	x		0.696	0.644	
	y		1/2	1/2	
H <sub>2</sub> O(3)	occ.		0.42	0.90	
	x		1/2	1/2	
	y		1/2	1/2	
	z		1/2	1/2	
	occ.		0.48	0.64	

Notes: (1) Isotropic temperature factors fixed to  $B = 0.8$  for Mn, 1.0 for O, and 5.0 for H<sub>2</sub>O. Overall isotropic temperature factors were refined (see Table 2). (2) The estimated errors determined by the Rietveld refinements are typically 0.001 for Mn, 0.002 for O, and 0.006 for H<sub>2</sub>O. The actual errors are probably several times these values, at least for the anions (see discussion of errors in text).

biased by the model structure, typically to a greater degree than in single-crystal experiments. This is because the observed Bragg intensities determined by the Rietveld program for overlapping peaks are assumed to have the same ratios as the corresponding calculated intensities. Consequently, the amount of information contained on the resulting difference-Fourier maps is typically less (and electron-density maxima are lower) than on comparable maps resulting from single-crystal data. For example, difference maps calculated for analcime (Bish and Post, unpub. results), in the same manner as described for todorokite, show only 2 to 5  $e^{-}/\text{\AA}^3$  peaks for the Na and water sites. It is noteworthy, however, that for analcime all of the cavity species were accurately located on the maps, and there were no extra peaks larger than 0.5  $e^{-}/\text{\AA}^3$ .

All of the significant electron-density peaks ( $>0.3 e^{-}/\text{\AA}^3$

TABLE 4. Bond distances ( $\text{\AA}$ ) for todorokite

Mn1–O2 ( $\times 4$ )	1.82	Mn3–O5 ( $\times 4$ )	1.85
–O3 ( $\times 2$ )	1.75	–O6 ( $\times 2$ )	1.90
Mean	1.80	Mean	1.87
Mn2–O1 ( $\times 2$ )	1.95	Mn4–O1	1.90
–O2	1.89	–O4 ( $\times 2$ )	1.92
–O3 ( $\times 2$ )	1.94	–O5	2.05
–O4	1.98	–O6 ( $\times 2$ )	1.98
Mean	1.94	Mean	1.96
O1–O1	2.84	O4–O4	2.84
–O2	2.81	–O5	2.84
–O3	2.60	–O6	2.65
–O4	2.93		
–O4'	3.02	O5–O5	2.84
		–O5'	2.38
O2–O2	2.84	–O6	2.56
–O2'	2.28	–O6'	2.75
–O3	2.23		
–O3'	2.78	O6–O6	2.84
O3–O3	2.84		
–O4	2.88		
H <sub>2</sub> O(1)–O1	3.13	H <sub>2</sub> O(2)–O3	2.79
–O2	2.71	–O4	3.49
–O6	2.38	–O5	2.11
–H <sub>2</sub> O(1)	2.84	–H <sub>2</sub> O(2)	2.84
–H <sub>2</sub> O(3)	2.35	–H <sub>2</sub> O(3)	2.30
	H <sub>2</sub> O(3)–H <sub>2</sub> O(3)	2.84	

Note: Bond distances are calculated from atom positions determined for the  $K\alpha$  data set for the sample from South Africa. Errors as determined by the Rietveld refinement are about one in the last place, but as explained in the text, actual errors are probably several times larger.

$\text{\AA}^3$ ) on the difference maps for the three todorokite data sets are centered at levels  $y = 0$  and  $y = 1/2$  and are located in the tunnel region of the structure or near framework-atom positions. The Mn and O atoms in the  $[3 \times 3]$  framework also have  $y$  coordinates of 0 and  $1/2$  and are plotted for reference on the Fourier sections in Figures 4 and 5. Corresponding map sections for both samples are very similar, suggesting that they reveal real structural information rather than just artifacts. The most significant area of electron density in each map is centered at about (0.37, 0, 0.37); the peak for the Cuban material is slightly larger (2.3 vs. 1.8  $e^{-}/\text{\AA}^3$ ) and better defined than that for the South African sample. The next largest difference peaks are about 1.0 to 1.5  $e^{-}/\text{\AA}^3$  located at approximately ( $2/3$ ,  $1/2$ ,  $1/3$ ). The map for the South African  $K\beta$  data set shows a 1.5  $e^{-}/\text{\AA}^3$  peak at ( $1/2$ ,  $1/2$ ,  $1/2$ ), but the other two difference maps have peaks at that position that are only about half as large. Scatterings of small peaks occur in the vicinities of ( $2/3$ , 0,  $1/3$ ) and ( $1/3$ ,  $1/2$ ,  $1/3$ ) in all of the maps. The todorokite chemical formulae given above indicate approximately four water molecules per unit cell; thus most of the electron density in the tunnels must be due to water, which probably explains some of the diffuseness of the difference peaks.

For the remainder of the Rietveld refinement process, all of the tunnel cation species were assumed to be water. Water sites were included in the todorokite structure model, corresponding to the major areas of electron density on the difference maps (see Table 3). The temperature

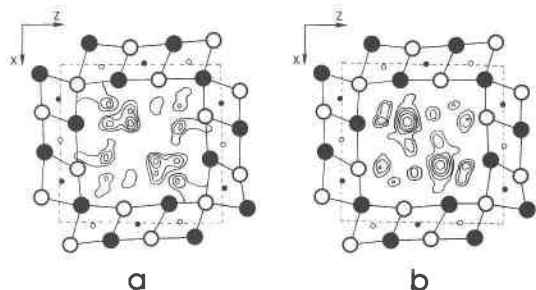


Fig. 4. Difference-Fourier maps at  $y = 0$ , superimposed onto projections of the todorokite framework looking down  $b$  ( $\beta = 90^\circ$ ), for samples from (a) South Africa ( $K\alpha$ ), and (b) Cuba. The maps were calculated using the DLS framework and Rietveld-derived observed Bragg intensities. The filled circles represent atoms at  $y = 0$ , and the open circles, those at  $y = 1/2$ . The large circles indicate O and the small circles Mn atoms. The contour interval is  $0.4 \text{ e}^-/\text{\AA}^3$ . The unit cell is indicated by the dotted lines.

factors for the water positions were fixed to  $B = 5.0$ , and the positions and occupancy factors were refined along with the profile parameters. When we attempted to refine isotropic temperature factors for the water positions, they increased to very large values ( $B > 10$ ), especially for  $\text{H}_2\text{O}(2)$ . This might in part result from high correlations with occupancy factors. Yet, in Rietveld refinements, temperature parameters can implicitly correct for other problems of an experimental nature associated with the data set, so they may be suspect. It is also likely, however, that the large temperature factors are indicating a large degree of positional disorder on the water sites, similar to what is observed in many zeolite structures, where  $B$  values for water sites are commonly  $> 10$  (e.g., Rinaldi et al., 1974, where  $B$  values for phillipsite ranged from 7 to 19).

Inclusion of the water sites in the refinements significantly reduced the  $R_{wp}$  values (by 0.04 to 0.05). Results for the South Africa  $K\alpha$  data indicate that the  $\text{H}_2\text{O}(1)$  site has the largest occupancy; however, the  $K\beta$  refinement locates a slightly different position for  $\text{H}_2\text{O}(1)$  and assigns nearly equal occupancies to  $\text{H}_2\text{O}(1)$  and  $\text{H}_2\text{O}(2)$ . The  $\text{H}_2\text{O}(2)$  positions are also slightly different among the three cases. We did not attempt to refine water sites for each of the several small peaks shown on the difference maps in the region around  $\text{H}_2\text{O}(2)$ . Each of the refinements show about 0.4 to 0.6 water molecules at  $(1/2, 1/2, 1/2)$  and nothing at  $(2/3, 0, 1/3)$ . The slightly different water positions resulting from the various data sets are most likely a consequence of the smeared-out nature of the tunnel electron density.

In the final stages of refinement, the positions of Mn and O atoms were allowed to vary along with the water positions and occupancy factors and profile parameters (total variables = 36). Individual isotropic temperature factors were held fixed to  $B = 0.8$  for Mn and  $B = 1.0$  for O atoms. Final observed and calculated profiles for the South African  $K\alpha$  refinement are compared in Figure 3. The final residuals and atomic parameters are listed in Tables 2 and 3, respectively, and bond distances are listed

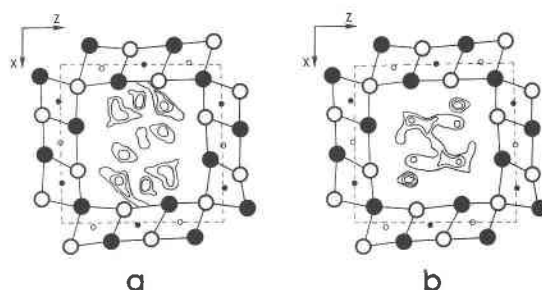


Fig. 5. Difference-Fourier maps at  $y = 1/2$ . For further explanation, see Fig. 4 caption.

in Table 4. The refined Mn positions resulting from the three data sets agree quite closely, therefore giving us confidence in their accuracy. The general agreement among the O-atom positions for the various refinements is also reasonably good although they show more variation than the Mn positions, especially the O5 determined for the Cuban data. Most of the variation among the sets of refined atom positions probably is caused by disorder and/or minor preferred orientation in the samples. Slight differences in atom positions in the two samples are expected because of differences in composition and unit-cell parameters. Atom positions determined using the  $K\alpha$  data set from South Africa were used to calculate the bond lengths in Table 4 because this refinement yielded the lowest profile and Bragg residuals. The slightly higher residuals for the South African  $K\beta$  profile probably result from the much lower count rates (approximately 40 cps for the largest peak) and poorer counting statistics.

## DISCUSSION

The refinement results are consistent with the  $[3 \times 3]$  tunnel structure proposed by Turner and Buseck (1981), and the final Mn,O atom positions compare quite well with the DLS model of the octahedral framework (Table 3). Unfortunately, it is difficult to assess the accuracy of our refined todorokite atom positions and, consequently, bond distances. The estimated errors determined by the Rietveld refinement are based on counting statistics in the data but do not account for errors in the profile functions, nor for sample-related problems such as preferred orientation and structural disorder. In particular, we have found that atomic coordinates can be significantly affected by preferred orientation of crystallites in the sample. For example, refinements that we have carried out on hollandite and romanechite (Post and Bish, in prep.) show that greatly improved fits are obtained between Rietveld and single-crystal results when preferred orientation is minimized (by grinding samples to smaller particle sizes and by side-loading sample holders). It appears that the largest effect of nonrandom samples is on the positions of the light elements such as oxygen; for both romanechite and hollandite, the Rietveld-refined Mn positions are not significantly different from the values determined by single-

crystal refinements. As mentioned above, the todorokite powder patterns do not show evidence of significant preferred orientation problems; however, the possibility of minor effects cannot be dismissed.

### Octahedral framework

The Mn–O distances resulting from the Rietveld refinement of romanechite (which has a structure similar to that of todorokite and also exhibits disorder) agree with single-crystal values to within 0.10 Å or less; most agree within 0.05 Å. It is probably reasonable to assume that the todorokite distances in Table 4 have similar uncertainties. For the most part, the todorokite Mn–O distances fall within the range (1.87–2.12 Å) shown by single-crystal studies on romanechite, hollandite, and cryptomelane (Post et al., 1982; Turner and Post, in prep.). The distances in the Mn1 octahedron, however, are anomalously short and probably reflect errors in the refinement.

Although it is not possible to discuss precise details of the todorokite framework because of the uncertainties in the bond distances, some general characteristics are evident. For example, the average Mn2–O and Mn4–O bond lengths (1.94 and 1.96 Å, respectively) are considerably longer than the mean Mn1–O and Mn3–O distances (1.80 and 1.87 Å, respectively), suggesting that the larger lower-valence cations, e.g., Mn<sup>3+</sup> and Mg<sup>2+</sup> (necessary to offset the charges on the tunnel cations), preferentially occupy the Mn2 and Mn4 octahedral sites. This is consistent with single-crystal results for romanechite that show Mn<sup>3+</sup> ordering into the octahedral sites at the edges of the triple chains (Post and Turner, 1986). Similarly, a recent refinement of a synthetic [2 × 5] tunnel manganese oxide structure (Tamada and Yamamoto, 1986) shows the largest octahedra to be at the edges of the quintuple chain. Presumably, the larger Mn2 and Mn4 sites also accommodate cations such as Cu<sup>2+</sup>, Co<sup>2+</sup>, and Ni<sup>2+</sup> that commonly occur in todorokite (Ostwald, 1986). According to the chemical analysis of the todorokite from South Africa, if all of the Mg cations are in the Mn2 or Mn4 octahedra, they fill approximately 10% of those sites. Using typical Mn<sup>4+</sup>–O and Mg<sup>2+</sup>–O distances of 1.91 and 2.10 Å (Shannon, 1976), respectively, one calculates for these sites an average cation–O bond length of 1.93 Å, compared to 1.94 and 1.96 Å in Table 4. The slightly longer refined distances suggest that perhaps the experimental distances are in error or that Mn<sup>3+</sup> also is present in the sites. Without knowing the amount of hydroxyl in the structure, if any, and the distribution of Mg between the tunnel and octahedral positions, it is not possible to calculate exactly the amount of Mn<sup>3+</sup> in the framework. The Mn2 and Mn4 octahedra do not, however, show significant evidence of Jahn-Teller distortion that should accompany large amounts of Mn<sup>3+</sup> on these sites.

The Mn2 and Mn4 positions (see Fig. 1) are shifted from the centers of their coordination octahedra, away from the Mn1 and Mn3 cations, respectively. Similar shifts are observed in romanechite (Turner and Post, in prep.) and hollandite (Post et al., 1982) and probably serve to

minimize repulsive forces between neighboring Mn cations.

In all of our discussions we have assumed that the Mg cations are in octahedral sites and the Na, K, Ca, Ba, Sr, and water are in the tunnels. Cation-exchange experiments using the sample from Cuba show that Ba and Sr replace some of the Ca but not Mg (Bish and Post, in prep.), consistent with the notion that Mg is not in the tunnels. Furthermore, six-coordination is typical for Mg in most other minerals. In the samples used for this study, there is sufficient Mg in the octahedral sites such that Mn<sup>3+</sup> is not needed for charge balance, unless significant amounts of hydroxyl anions are present in the structures. The presence of Mg and/or Cu, Ni, Co, etc., instead of Mn<sup>3+</sup> as the lower-valence octahedral cation perhaps serves to stabilize todorokite under conditions in which Mn<sup>3+</sup> cannot exist (Burns et al., 1983), e.g., highly oxidizing environments.

### Tunnel water and cations

The difference-Fourier maps in Figures 4 and 5 and the subsequent refinements show a major area of electron density in the tunnels at about (0.38, 0, 0.38) that we tentatively identify as water, which is known to be the major tunnel species. The distance of this site from the nearest O atoms is about 2.40 Å, which is slightly short compared to typical O–O(water) distances. The refined H<sub>2</sub>O(2) position is only 2.11 Å from O5. The difference map, however, suggests a great deal of positional disorder over these sites, thus making it difficult to determine exact bond distances. The disorder possibly arises from various arrangements of lower-valence cations over the octahedral sites and/or different  $\beta$  angles in different unit cells (as observed in HRTEM studies). Structure-energy calculations for hollandite minerals show clearly that the positions of the tunnel cations in these structures are a function of the configuration of the lower-valence octahedral cations surrounding the tunnel sites in a given unit cell (Post and Burnham, 1986a). Also, the chemical formulae for most todorokite samples show several kinds of tunnel cations, all with occupancies less than one. Therefore, the tunnel contents of various unit cells are different, which undoubtedly contributes to the positional disorder. Furthermore, the actual water positions might be displaced off of the mirror planes, which would result in longer H<sub>2</sub>O–O bond lengths. Structure-energy calculations, described below, in fact indicate that this is likely the case.

Preliminary structure-energy calculations support the assumption that the electron density at about (0.36, 0, 0.35) [H<sub>2</sub>O(1)] is due to water. Calculations using the computer program WMIN (Busing, 1981) and modified electron-gas short-range energy terms (Post and Burnham, 1986b) yield minimum-energy water positions at about (0.37, 0.03, 0.37), regardless of the lower-valence cation arrangement on the octahedral sites or the number of water molecules and cations in the tunnels. The models with four water molecules per unit cell (typical todorokite analyses show 3.2 to 4.5 water molecules per cell) deter-

mine a second minimum-energy position at about (0.6, 0.6, 0.4). The difference maps in Figure 5 show electron density in this region of the tunnel, and the refinement of the South African  $K\alpha$  data yielded a tunnel position at (0.7, 0.5, 0.38) [ $\text{H}_2\text{O}(2)$ ] with an occupancy slightly less than that of  $\text{H}_2\text{O}(1)$ . The  $K\beta$  refinement placed  $\text{H}_2\text{O}(2)$  at (0.64, 0.5, 0.39). The calculations consistently show the second water site 0.1 to 0.6 Å off of the mirror plane at  $y = 1/2$ . Structure-energy minimizations with Ca and Na cations along with the water indicate that the cations occupy a range of positions in the center of the tunnel near  $(1/2, 1/2, 1/2)$ , depending on the number of water molecules in the tunnel and the arrangement of lower-valence cations in the octahedral framework. Such a positionally disordered site is consistent with the Fourier maps showing smeared-out electron density and the refinement of a small occupancy factor (0.5 O atoms) at  $(1/2, 1/2, 1/2)$ .

The above description of the water positions in the todorokite tunnels is consistent with infrared spectroscopy studies of todorokite (Potter and Rossman, 1979) indicating the presence of water molecules in several well-defined crystallographic sites and, in addition, a disordered water component. If, as the energy calculations suggest, the tunnel cations are near  $(1/2, 1/2, 1/2)$  and  $\text{H}_2\text{O}(1)$  and  $\text{H}_2\text{O}(2)$  are fully occupied in a given unit cell, then the cations are octahedrally coordinated by the water molecules. The distances from  $\text{H}_2\text{O}(1)$  to  $(1/2, 1/2, 1/2)$  are approximately 2.30 to 2.35 Å, which are reasonable for (Ca,Na)-O bond lengths. The larger K and Ba, on the other hand, might occupy positions near the walls of the tunnels, perhaps accounting for some of the smaller difference peaks in Figures 4 and 5. The multiple peaks evident on the difference maps in the vicinities of the refined water sites probably represent different water (and/or cation) positions, depending on the type of tunnel cation (if any), the number of water molecules, and the configuration of lower-valence octahedral cations in a given unit cell. The difference maps and the energy calculations indicate that the most favorable and well-defined water position [ $\text{H}_2\text{O}(1)$ ] is in the more open corner of the tunnel. Most likely, only after this larger site is filled do water molecules occupy other tunnel positions.

#### BIRNESSITE TO TODOROKITE TRANSFORMATION

Recently, Golden et al. (1986, 1987) synthesized todorokite by heating birnessite under saturated steam pressure at 155 °C. Several observations support their suggestion that birnessite might also be the precursor to most natural todorokite. One of these is the trilling pattern formed by twinned fibers that is observed in electron-microscope images and is almost diagnostic of todorokite. This twinning is readily explained in the context of a birnessite to todorokite transformation. Assuming that the todorokite tunnels form by constructing triple-chain walls that connect adjacent MnO octahedral sheets in birnessite, then any of three different orientations of tunnels can result, at 120° to each other, in different layers because of the threefold symmetry of the octahedral sheets.

This is consistent with electron-microscope photographs of todorokite showing stacked layers in which the tunnels in any given layer are oriented in one direction but are rotated 120° relative to tunnels in other layers (Turner and Buseck, 1981).

A birnessite parent also explains why the chain-width disorder (e.g., quadruple, quintuple, etc., chains) observed in HRTEM photographs of todorokite (Chukhrov et al., 1978; Turner and Buseck, 1981) occur only in one crystallographic direction ( $\parallel a$ ). The direction of disorder is parallel to the original birnessite octahedral sheets. During the transformation to todorokite, some tunnels other than  $[3 \times 3]$  form (e.g.,  $[3 \times 4]$ ,  $[3 \times 5]$ , etc.), and, because the original layer separation in birnessite constrains one dimension of the tunnels, larger chain widths can form only along the layer direction.

Considering the approximately 7-Å spacing of the octahedral layers of birnessite versus the 9.6-Å separation between triple chains in todorokite, it is necessary for the birnessite structure to expand to essentially a busierite structure (layer spacing of about 9.6 Å) before transforming to todorokite. In fact, experiments by Golden et al. (1986) indicate that synthetic birnessite easily hydrates to busierite in an aqueous environment, suggesting that the actual transformation, therefore, is busierite (which might or might not have formed from birnessite) to todorokite.

#### SUMMARY

Rietveld refinements, using X-ray powder data, of the structures of two todorokite samples have confirmed the basic  $[3 \times 3]$  tunnel structure and have provided, for the first time, information about the positions of the tunnel cations and water molecules. Fourier-difference maps reveal a major tunnel water and/or cation position at (0.37, 0, 0.35), along with other sites near (0.70,  $1/2$ , 0.38) and  $(1/2, 1/2, 1/2)$ . Structure-energy calculations suggest that cations such as Na and Ca reside near  $(1/2, 1/2, 1/2)$ , where they are octahedrally coordinated by water molecules occupying the other two tunnel positions. Considerable positional disorder on the tunnel sites probably arises from different arrangements of lower-valence octahedral cations in different unit cells and from variety in the tunnel contents.

The refined Mn-O bond distances indicate that the octahedra on the edges of the triple chains are larger than those in the middle and therefore likely accommodate the larger, lower-valence cations, e.g.,  $\text{Mg}^{2+}$ ,  $\text{Mn}^{3+}$ ,  $\text{Cu}^{2+}$ ,  $\text{Ni}^{2+}$ , etc.

The formation of todorokite from a birnessite or busierite parent is consistent with the trilling twin pattern observed in most todorokite and with the HRTEM observation of chain-width disorders occurring in only one crystallographic direction.

#### ACKNOWLEDGMENTS

We are grateful to Ray Young and Scott Howard for assistance with the DBW3.2 computer program.

## REFERENCES CITED

- Baerlocher, Ch. (1984) The possibilities and limitations of the powder method in zeolite structure analysis: The refinement of the silica end-member of TPA-ZSM-5, Proceedings of the 6th International Zeolite Conference, Reno.
- Baerlocher, Ch., Hepp, A., and Meier, W.M. (1977) DLS-76. Institut für Kristallographie und Petrographie, ETH, Zurich.
- Bish, D.L., and Post, J.E. (1984) Thermal behavior of todorokite and romanechite. Geological Society of America Abstracts with Programs, 16, 625.
- Burns, R.G., and Burns, V.M. (1977) The mineralogy and crystal chemistry of deep-sea manganese nodules, a polymetallic resource of the twenty-first century. In *Mineralogy: Towards the 21st Century* (Centenary Volume, Mineralogical Society, London, p. 49-67), Philosophical Transactions of the Royal Society of London, A286, 283-301.
- Burns, R.G., Burns, V.M., and Stockman, H.W. (1983) A review of the todorokite-buserite problem: Implications to the mineralogy of marine manganese nodules. *American Mineralogist*, 68, 972-980.
- Busing, W.R. (1981) WMIN, a computer program to model molecules and crystals in terms of potential energy functions. U.S. National Technical Information Service, ORNL-5747.
- Chukhrov, F.V., Gorshkov, A.I., Sivtsov, A.V., and Berezovskaya, V.V. (1978) Structural varieties of todorokite. *Izvestia Akademia Nauk, SSSR, Series Geology*, 12, 86-95.
- Giovanoli, R., and Burki, P. (1975) Comparison of X-ray evidence of marine manganese nodules and nonmarine manganese ore deposits. *Chimia*, 23, 470-472.
- Golden, D.C., Chen, C.C., and Dixon, J.B. (1986) Synthesis of todorokite. *Science*, 231, 717-719.
- (1987) Transformation of birnessite to buserite, todorokite, and manganite under mild hydrothermal treatment. *Clays and Clay Minerals*, 35, 271-280.
- Hill, R.J. (1984) X-ray powder diffraction profile refinement of synthetic hercynite. *American Mineralogist*, 69, 937-942.
- Hill, R.J., and Madsen, I.C. (1984) The effect of profile step counting time on the determination of crystal structure parameters by X-ray Rietveld analysis. *Journal of Applied Crystallography*, 17, 297-306.
- Ostwald, J. (1986) Some observations on the chemical composition of todorokite. *Mineralogical Magazine*, 50, 336-340.
- Post, J.E., and Burnham, C.W. (1986a) Modeling tunnel-cation displacements in hollandites using structure-energy calculations. *American Mineralogist*, 71, 1178-1185.
- (1986b) Ionic modeling of mineral structures in the electron gas approximation: TiO<sub>2</sub> polymorphs, quartz, forsterite, diopside. *American Mineralogist*, 71, 142-150.
- Post, J.E., and Turner, S. (1986) Structure refinement of romanechite; Subcell and supercell. 14th International Mineralogical Association Meeting Abstracts, p. 203.
- Post, J.E., Von Dreele, R.B., and Buseck, P.R. (1982) Symmetry and cation displacements in hollandites: Structure refinements of hollandite, cryptomelane, and priderite. *Acta Crystallographica*, B38, 1056-1065.
- Potter, R.M., and Rossman, G.R. (1979) The tetravalent manganese oxides: Identification, hydration, and structural relationships by infrared spectroscopy. *American Mineralogist*, 64, 1199-1218.
- Rietveld, H.M. (1969) A profile refinement method for nuclear and magnetic structures. *Journal of Applied Crystallography*, 2, 65-71.
- Rinaldi, R., Pluth, J.J., and Smith, J.V. (1974) Zeolites of the phillipsite family. Refinement of the crystal structures of phillipsite and harmotome. *Acta Crystallographica*, B30, 2426-2433.
- Shannon, R.D. (1976) Revised effective ionic radii and systematic studies of interatomic distances in halides and chalcogenides. *Acta Crystallographica*, A32, 751-767.
- Stewart, J.M. (1976) The X-ray system of crystallographic programs. Technical Report TR-445, Computer Science Center, University of Maryland, College Park.
- Tamada, O., and Yamamoto, N. (1986) The crystal structure of a new manganese dioxide (Rb<sub>0.27</sub>MnO<sub>2</sub>) with a giant tunnel. *Mineralogical Journal*, 13, 130-140.
- Thompson, P., and Wood, I.G. (1983) X-ray Rietveld refinement using Debye-Scherrer geometry. *Journal of Applied Crystallography*, 458, 458-472.
- Turner, S. (1982) A structural study of tunnel manganese oxides by high-resolution transmission electron microscopy. Ph.D. thesis, Arizona State University, Tempe.
- Turner, S., and Buseck, P.R. (1979) Manganese oxide tunnel structures and their intergrowths. *Science*, 203, 456-458.
- (1981) Todorokites: A new family of naturally occurring manganese oxides. *Science*, 212, 1024-1027.
- Villiger, H. (1969) DLS-Manual. Institut für Kristallographie und Petrographie, ETH, Zurich.
- Wiles, D.B., and Young, R.A. (1981) A new computer program for Rietveld analysis of X-ray powder diffraction patterns. *Journal of Applied Crystallography*, 14, 149-151.

MANUSCRIPT RECEIVED OCTOBER 19, 1987

MANUSCRIPT ACCEPTED MARCH 18, 1988